Validation of an Adaptive Temperature Model for Closed Microalgae Cultivation Systems

Ali Gharib, W. Djema, P. Moñino Fernández, R. Chin-On, M. Janssen, Olivier Bernard

Validation of an Adaptive Temperature Model for Closed Microalgae Cultivation Systems

A. Gharib[a], W. Djema[a], P. Moñino Fernández[b], R. Chin-On[b], M. Janssen[b], O. Bernard[a]

[a]*Centre Inria d'Université Côte d'Azur Méditerranée, BIOCORE Project-Team, Université Nice Côte d'Azur, 2004, Route des Lucioles BP 93, Valbonne, 06902, Sophia-Antipolis Cedex, France*
[b]*Bioprocess Engineering, AlgaePARC, Wageningen University & Research, P.O. Box 16, Wageningen, 6700 AA, the Netherlands*

Abstract

Accurate temperature prediction plays a crucial role in optimizing microalgae growth conditions. For that, we recently developed a generic adaptive temperature prediction model, called the *Simplified Auto Tuning Heat Exchange (SATHE)* model, which was initially tailored to open raceway ponds. In this study, we adapt and validate the SATHE model specifically for the case of closed reactors. We assess two distinct closed reactor types across different geographical locations: a tubular photobioreactor situated in a greenhouse in Wageningen (Netherlands) and a flat panel reactor on Bonaire, a Caribbean island in the Lesser Antilles. Finally, we discuss the practical applications of our model. We test the reactors' performance in different geographical settings and assess energy consumption under varied meteorological conditions. This paper highlights the versatile model's potential for optimizing closed-reactor operation and thermal management in various geographical locations.

Keywords: Modelling, Temperature, Validation, Nonlinear, Dynamical systems.

1. Introduction

Microalgae are microscopic photosynthetic organisms that convert sunlight and carbon dioxide into valuable biomass, offering potential applications in biofuel production, wastewater treatment, and as a source of high-value

compounds like omega-3 long-chain polyunsaturated fatty acids, pigments or antioxidants (Jacob-Lopes et al., 2020, Kumar et al., 2020). Maximizing microalgae productivity is crucial for achieving maximal biomass yield. Constraints in productivity can stem from factors like nutrient availability, reactor design, and metabolic processes. Notably, physical factors, especially light availability and temperature conditions, directly impact photosynthesis, exerting a significant influence on microalgae growth (Singh and Singh, 2015). Temperature is a major factor, as it directly influences the enzyme activities within the metabolism, and thus growth rate and cell composition. High temperatures (above the optimum growth temperature) lead to the denaturation of some key proteins eventually increasing the mortality rate (Serra-Maia et al., 2016). The temperature of the culturing device must then stay in a range compatible with the thermal niche of the produced species to maintain productivity (Ras et al., 2013).

Closed systems photobioreactor (PBR), give precise control over the cultivation environment, leading to higher productivity and improved photosynthesis (Huang et al., 2017, Ruiz et al., 2016, Wang et al., 2012). Tubular and flat panel reactors in particular are (the most) popular choices, considering that the required light source is free (does not incur any direct costs for its use as an energy source) and readily available (Borowitzka, 1999). PBRs, however, have the drawback that they are more sensitive to overheating due to their low thermal inertia (Pruvost et al., 2016). Without a temperature control system, the temperature is even likely to reach lethal values for the cells.

Accurately predicting reactor temperature in PBR is thus crucial to simulate microalgae growth, strain compatibility, reactor design, or energy consumption, and to support algorithms and control strategies to avoid overwarming. Heat transfer models in the literature have demonstrated remarkable accuracy in predicting temperatures in open raceway ponds (Béchet et al., 2011, Casagli and Bernard, 2022). Heat transfer models for PBR are more rare in the literature, generally developed for the simpler flat panels, and rarely validated on horizons longer than a week (Goetz et al., 2011, Todisco et al., 2022). Nevertheless, these models require an in-depth understanding of the particular cultivation system, including its geometry, technical intricacies, and a broad spectrum of physical parameters. Consequently, customizing these specific models and identifying their parameters for each reactor configuration presents a challenging and time-consuming process.

Based on the heat transfer model developed by Casagli and Bernard

(2022), we have recently introduced the SATHE model tailored for temperature predictions within microalgae cultivation systems (Gharib et al., 2024). By retaining the fundamental structure of the most influential terms while streamlining them, we have created a refined model with reduced complexity, characterized by 6 parameters for identification instead of 27. Thereby we are turning the complex heat transfer modelling problem into an identification problem. This clear and simple structure of the model empowers the adaptability to various reactors, facilitated by a gradient-driven calibration phase utilizing a dataset from actual measurements (Gharib et al., 2023).

In Gharib et al. (2023) we validated the model only with raceway reactors. This study shows that the SATHE model can accurately represent temperature inside microalgae cultivation systems, that differ strongly in their geometries and geographical positions, after a calibration procedure relying on dedicated algorithms to identify model parameters. We demonstrate the model's performance and its potential applications. This includes simulating temperature variations in different locations and exploring potential energy consumption across various regions and weather conditions.

The paper is structured as follows. In Section 2, we revisit the generic temperature model, analyzing its components and outlining our approach to identifying the model's parameters. Sections 3 and 4 present the validation of the model adapted to two closed PBRs, a tubular photobioreactor (TBR) based in Wageningen, Netherlands (Abiusi et al., 2022, Moñino Fernández et al., 2023) and a so-called V-shape reactor, based in Bonaire (Caribbean island) (Chin-On et al., 2022). We describe the reactors and the differences that will be significant from a modelling perspective and then present the validation results. Following that, Section 5 comprises the discussion, exploring potential applications and advantages of the SATHE model temperature prediction.

2. Methods

2.1. Presentation and analysis of the SATHE model for open raceway ponds

In this section, we revisit the SATHE model introduced in Gharib et al. (2023) and Gharib et al. (2024). This generic model is meant to describe the evolution of both the temperature T_p and the culture depth h in various types of reactors from open raceways to closed PBRs. It describes the temperature dynamics as the result of various heat fluxes, such as convection with air and

conduction with the ground, radiation from the medium, from air and from sunlight, evaporation and heat flow from the incoming medium.

It relies on weather data or forecasts, covering the values of air temperature T_a (K), relative humidity η $(-)$, light intensity $I_0(\mathrm{W\,m^{-2}})$, wind speed v_0 $(\mathrm{m\,s^{-2}})$, and the rain q^r $(\mathrm{m^3\,m^{-2}\,s^{-1}})$ as well as the inflow and outflow rate q^{in} and q^{out} $(\mathrm{m^3\,s^{-1}})$.

The dynamics of the model described in Gharib et al. (2023) and Gharib et al. (2024) are governed by,

$$\begin{aligned}\dot{T_p} = S_R \Big(&\theta_1 A(T_p) + \theta_2 B({T_p}^4) + \theta_3 C(T_a) + \theta_4 D({T_a}^4) \\ &+ \theta_5 E(I_0) + \theta_6 F(T_p, T_a, v_0, \eta) \\ &+ Q_{flow}(T_p, q^{in})\Big)/V \end{aligned} \tag{1a}$$

$$\dot{h} = \theta_6 q_{flow,ev} + q^{in}/S_R - q^{out}/S_R + q^r \tag{1b}$$

with

$$A(T_p) = \lambda_1\ T_p \tag{1c}$$

$$B(T_p) = \lambda_2\ T_p^4 \tag{1d}$$

$$C(T_a) = \lambda_3\ T_a \tag{1e}$$

$$D(T_a) = \lambda_4\ {T_a}^4 \tag{1f}$$

$$E(I_0) = \lambda_5\ I_0 \tag{1g}$$

$$F(T_p, T_a, v_0, \eta) = \lambda_6\ v_0^{0.8}(P(T_p) - \eta\ P(T_a)) \tag{1h}$$

$$P(\zeta) = \lambda_8\ exp(\lambda_9 + \ \lambda_{10}(\zeta + \lambda_{11})^{0.5})/\zeta$$

$$Q_{flow}(T_p, q^{in}) = (q^{in} + q^r)(T_a - T_p) - \ T_p\ \theta_6\ S_R q_{flow,ev} \tag{1i}$$

$$q_{flow,ev} = \lambda_7\ F\,(T_p, T_a, v_0, \eta) \tag{1j}$$

where S_R is the surface of the reactor, V the volume (for a raceway pond $V = hS_R$), $q_{flow,ev}$ the evaporation rate per $\mathrm{m^2}$, and T_{in} is the temperature of the influent flow. When it is not measured, it is assumed to be equal to the air temperature. For further information about the variables and values, we refer to (Gharib et al., 2024). The values of the nominal constants λ_i (see Casagli and Bernard (2022)), are provided in Table. 1. The adaptation of these constants to each case study is carried out with the constant θ_i. The θ_i are equal to 1 for the exact case described by Casagli and Bernard (2022). They are fine-tuned to fit a different case study, expecting their value never

to be far from 1, if the provided values for the surface S_R and the volume V_R are close to the reference situation. By adjusting the parameters θ_j's, with $j \in \{1, \ldots, 6\}$, in (1), the model can better align with the actual system behaviour, compensating for the simplifications made and enhancing the accuracy of predictions. Note also that the θ_j compensate for the computation of the actual surface which is submitted to the radiations. With complex geometries, the fraction of the reactor surface which is indeed enlighten can be difficult to determine due to the shadowing by other parts of the reactor or by external elements such as the building. The same applies for most of the heat fluxes, for which only a fraction of the reactor surface is active.

λ_i	value	λ_i	value
λ_1	-2.0093e-06 ($\mathrm{m\,s^{-1}}$)	λ_7	0.0017 ($\mathrm{K^{-1}}$)
λ_2	-1.3184e-14 ($\mathrm{m\,s^{-1}\,K^{-3}}$)	λ_8	1.0350 (-)
λ_3	2.0093e-06 ($\mathrm{m\,s^{-1}}$)	λ_9	0.97608 (-)
λ_4	1.0547e-14 ($\mathrm{m\,s^{-1}\,K^{-3}}$)	λ_{10}	-230.543 (-)
λ_5	2.3372e-07 ($\mathrm{m^3\,K\,J^{-1}}$)		
λ_6	-2.6203e-06 ($\mathrm{K^2\ Pa^{-1}m^{0.2}s^{-0.2}}$)		

Table 1: Values of the constants λ_i, i=1,...,10, derived from Casagli and Bernard (2022), Gharib et al. (2023)

The number of parameters to be determined reduces significantly to 6 in the case of the SATHE model, in contrast to the 27 parameters required by the heat-transfer model from Casagli and Bernard (2022). Additionally, the development of the SATHE model resulted in a reduction of one state (Gharib et al., 2024). We refer to Gharib et al. (2023, 2024) for further details on the model and its parameters.

The SATHE model incorporates seven essential terms describing temperature dynamics. In the following, we explain these terms and clarify their potential considerations for different (open) reactor configurations. The terms (1c) and (1e) represent the reactor convection term. They are separated in two different terms to enable the prediction of the convection rate specifically within a greenhouse, without needing to predict the temperature inside the greenhouse. This enhancement expands the model's applicability to reactors situated within a greenhouse environment.

Similarly, the term (1d) characterizes radiation from the reactor medium temperature, while (1f) represents the air radiation term. The term (1g) covers the solar radiation term. Originally tailored for a horizontal flat surface,

the adaptive nature of this term enables the representation of solar radiation for various reactor geometries. In addition to geometry, different reactor surface materials must account for light scattering, diffusion, and shading effects.

Additionally, inaccuracies may arise in air temperature data and incoming light sourced from weather stations that are geographically located not close to the reactor's position. Further, (1h) embodies the evaporation term, significantly influencing both temperature and liquid evaporation. It closely aligns with the first principle calculation of evaporation, emphasizing its critical impact on the system.

All heat transfer terms discussed so far are contingent upon parameters related to reactor configuration, dimensions, and, for closed reactors, material properties that influence terms based on the reactor covering's material and dimensions. These heat transfer terms depend on factors such as reactor design, size, and material properties. This is especially important for closed reactors, where materials and dimensions of the reactor covering play a significant role.

The final term (1i) provides a first principle representation of incoming flow heat, serving as a representative factor applicable to a wide array of reactor types, presuming knowledge of the inflow temperature. In the next section, we show how the SATHE model can be further simplified for closed PBR.

2.2. Introducing the SATHE model for closed PBR

For closed PBR the interplay between air and medium within the reactor is minimal. Representing the first principles, there is still a convective heat flow between the solution and the glass/wall of the reactor and another convective heat flow between the glass and the outside (air) like it has been done by Goetz et al. (2011). Nevertheless, accounting for these heat transfers involves additional state dynamics for the glass temperature and additional terms. These terms have structures which are the sum of slowly varying terms (*e.g.*, due to the evolution of the ground temperature for the conduction flux), or that are linear with respect to θ_1 (like the conducto-convective flux between water and concrete) which will be compensated by the linear term (1d) in the generic model. Also, the fraction of the surface area S_R which is affected by the various conductive, convective or radiative flux varies depending on the reactor geometry. These uncertainties are also

covered by multiplying S_R with the parameters θ_i in the SATHE model. Additionally, the inflow q_{in} is equal to the outflow q_{out} in (most) closed systems. As a result, the prediction model omits the state dynamics associated with depth/volume. The SATHE model for closed PBR can be described by

$$\begin{aligned} \dot{T}_R(T_R, T_a, I_0, \theta) = \quad & \Big(S_R \left(\theta_1 B(T_R^4) + \theta_2 D(T_a^4) + \theta_3 E(I_0)\right) + \\ & q_{in} \ (T_{in} - T_R) \Big) \tfrac{1}{V_R}, \end{aligned} \tag{2}$$

where T_{in} is the inflow temperature, S_R the surface of the PBR and V_R the liquid volume in the closed PBR.

For closed PBR that have no inflow the temperature dynamics can be described by

$$\dot{T}_R(T_R, T_a, I_0, \theta) = \quad \left(\theta_1 B(T_R^4) + \theta_2 D(T_a^4) + \theta_3 E(I_0)\right) \tfrac{S_R}{V_R}. \tag{3}$$

The number of parameters, to be identified reduces even more (from 6 to 3) compared to the SATHE model for open raceway ponds.

2.3. Identification

As previously mentioned, each reactor type introduces unique variations in these terms. To facilitate model adaptation with minimal data requirements, each term is rescaled from its nominal value by a parameter θ_i. This allows the model to be flexibly adjusted with a limited dataset, enabling accurate prediction of the medium-temperature.

Our observations reveal that with just four days of recorded weather data and internal reactor temperature, the SATHE model produces accurate predictions. Adding more data beyond this period does not (significantly) improve the model's predictions, but it reduces the uncertainty associated to the parameter estimation, and therefore the confidence interval of the prediction (Gharib et al., 2024, 2023).

The parameter adaptation process is executed through optimization, involving the minimization of squared temperature prediction errors. The theoretical problem is stated as

$$\min_{\theta \in \Theta} J(\theta) \tag{4a}$$

$$s.t. \qquad J(\theta) = \sum_{i=1}^{N_H} \left(\delta(t_i, \theta)\right)^2, \tag{4b}$$

$$\boldsymbol{\Theta} = \{\theta \in \Re^n \colon \theta_k \geq 0, k = 1, 2, \ldots n\} \tag{4c}$$

$$\delta(t_i, \theta) = y(t_i, \theta) - y_m(t_i), \quad \text{for } i \in 1, \ldots, N_H, \tag{4d}$$

where prediction errors δ are calculated as the difference between the predicted output $y(t_i, \theta)$ and the measured output y_m at each time instance t_i (or N_H steps), and n the number of parameters that have to be calibrated. The sole constraint, as outlined in (4c), is that the parameters must be positive. To perform this optimization, we employ the lsqnonlin toolbox in Matlab 2020, using the Levenberg-Marquardt algorithm for nonlinear least squares curve fitting. Leveraging analytical gradients improves parameter optimization in time and prediction accuracy (see appendices Appendix A and Appendix B).

Building upon the adaptive model's capabilities and its potential for identifying accurate parameter values, we now shift our attention to validating the model across two distinct reactors. To validate the temperature prediction performance, we calculate the Root Mean Squared Error (RMSE)

$$\text{RMSE}(\theta) = \sqrt{\frac{\sum_{i=0}^{N_H - 1} (\delta(t_i, \theta))^2}{N_H}} \tag{5}$$

and the Mean Absolute Error (MAE)

$$\bar{\delta}(\theta) = \frac{1}{N_H} \sum_{i=1}^{N_H} |\delta(t_i, \theta)| \tag{6}$$

over 1 day, 4 days, 14 days and till the end of the respective data sets. All results are listed in Table. 2.

The parameter uncertainty calculations and uncertainty predictions follow the approach in Gharib et al. (2024). Here, we assume a temperature measurement error with a standard deviation of $0.5°K$ and a confidence level of $\alpha = 90\%$.

3. Extending the SATHE Model to TBR

3.1. Description of the TBR

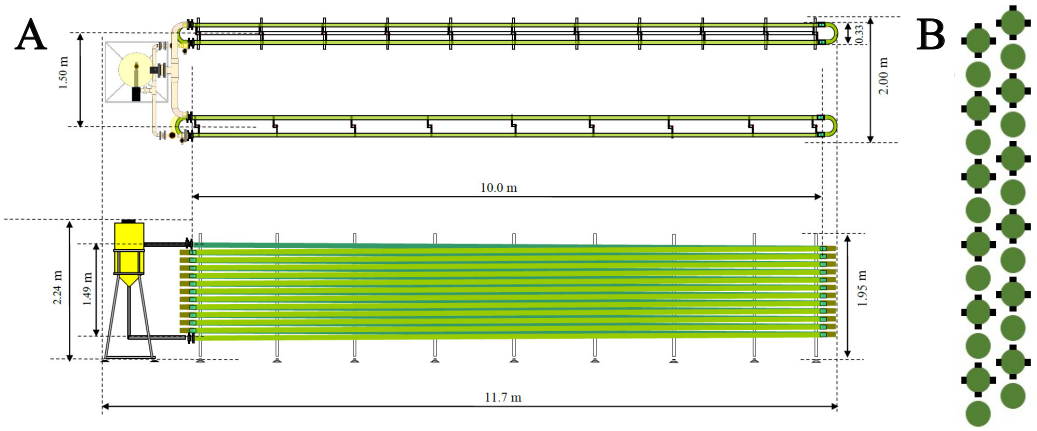

Figure 1: (A) Scheme of the LGem TBR from (top) top view and (bottom) side view (GemTube MK-1 1500s product spec., 2015). The reactor consists of two identical sets of tubes that act as solar collectors, connected to one circulator vessel (yellow). (B) Scheme of the light sensors located in the tubes of the right helix. Green circles represent a vertical cut of each of the tubes and black squares represent the sensors.

A three-dimensional tube reactor is a configuration characterized by multiple layers of vertically stacked tubes, creating a construction of vertical panels. Unlike its single-layer counterpart, the three-dimensional tube reactor mitigates issues related to high light intensity by placing tubes in each other's shade. This design optimization offers several advantages, such as increased areal productivity due to a higher tube density on the same horizontal surface, consequently enhancing the yield per square meter (Huang et al., 2017, Acién et al., 2017).

We use data from an experiment running on a pilot-scale PBR system, specifically the LGem TBR, featuring a two-phase TBR LGemTube MK-1 1500s (LGem, The Netherlands) (Alavijeh et al., 2020). This system comprises two identical sets of 867.5 L tubes, connected to a circulator vessel. Fig. 1 provides a schematic view, including principal dimensions. Each helix consists of 12 vertically stacked tubes with a 0.062 m diameter (external), totaling a tube length of 281 m. The reactor total liquid working volume was 1343 L, and online temperature and pH measurements were continuously monitored (Guimarães et al., 2021).

To assess light exposure, incidental light in the solar collector was meticulously measured using 48 sensors arranged in arrays of four within each of the 12 tubes of the right helix, offering comprehensive coverage (Fig. 1). The polyextremophilic red microalgae *Galdieria sulphuraria*, known for its adaptability to diverse environmental conditions, was cultivated in the PBR . This species thrives at low pH levels (0-4), temperatures up to 57 °C, and osmotic pressures up to $400\,\mathrm{g\,L^{-1}}$, making it a promising candidate for various biotechnological applications. The cultivation system maintained night temperature consistently around 27 - 27.5 °C in both systems, emphasizing the significance of thermophilic conditions for *G. sulphuraria*. This was achieved through the implementation of a heat exchanger to ensure optimal growth conditions during the night phase of the cultivation cycle. *G. sulphuraria*, thrives at elevated temperatures, and the maintenance of optimal night temperatures supports continuous growth. Modeling the temperature provides crucial insights into the optimal geographical positioning and control setup for a new TBR. For further explanation, we refer to Abiusi et al. (2022), Moñino Fernández et al. (2023).

Now, we shift our focus to the difficulties faced in implementing the adaptive model. We explain the complexities involved in simulating the dynamic interplay of factors governing microalgal cultivation within the controlled environment of the LGem TBR.

3.2. Explaining the hypothesis for the SATHE model to adapt to the TBR

In this section, we explain the hypothesis by employing the SATHE model for PBR (3) to the TBR in Wageningen. One significant challenge in employing the SATHE model arises from the characteristics of our TBR compared to a traditional raceway pond. The model is designed to operate using weather data obtained from local weather stations. However, it is important to note that the reactor is situated within a greenhouse environment. The temperatures inside the greenhouse can differ significantly from the outside conditions, as shown in Fig. 2. These variations are regulated by factors such as the opening and closing of windows, additional heating, and the greenhouse effect itself.

The recorded weather data is obtained from a weather station in Deelen, Netherlands, located approximately 17 km away from the reactor. This spatial separation introduces a degree of uncertainty, particularly concerning temperature and light conditions, which may differ from those experienced at the reactor location.

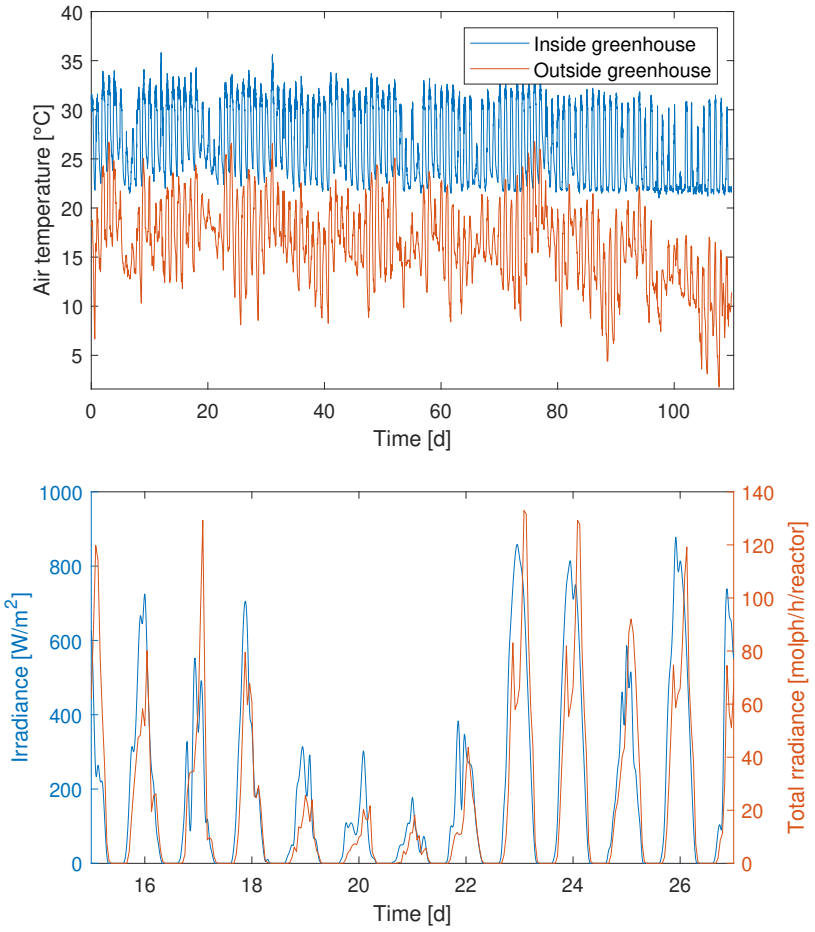

Figure 2: Upper graph: Temperature records in the greenhouse (blue) and from the weather station in Deelen. Lower graph: Irradiance comparison between the records of the weather station in Deelen for a flat surface (in W/m^2) and the total incoming irradiance per hour on the total reactor (in molph/h/reactor).

The variation in light conditions presents a substantial source of uncertainty. The SATHE model is derived from a heat-temperature model (see Casagli et al. (2021)) that incorporates a solar radiation term tailored for a raceway pond. A critical distinction is that a raceway pond has a flat geometry, resulting in incoming light hitting the surface directly matching the recorded values from the weather station. In contrast, the TBR's geometric design requires a more complex description. Calculating incident light for a TBR must also consider potential shading effects from adjacent tubes, structures, or any other obstructions that could obstruct direct sunlight. As shown in Fig. 2, there exists more than just a simple multiplicative relationship between the irradiance derived from weather recordings and the total incoming irradiance.

The TBR lacks an inflow and maintains (almost) a constant liquid volume of $V_{TBR} = 1.343\,\mathrm{m}^3$. However, an additional complexity arises from the fact that the TBR was equipped with a heat exchanger. This heating element is triggered below a specific temperature threshold. The control action is triggered based on that temperature threshold T_s (here 27.5 °C), as shown in Fig. C.12.

It is worth noting that while the heat exchanger serves a crucial purpose, its capacity is limited and there exists the possibility of the temperature dropping below the set-point. Therefore, we add a parameter θ_4, that provides a flexible threshold in the SATHE model.

These assumptions lead to the PBR temperature model equation given by:

$$\dot{T}_{TBR} = \phi(T_{TBR}, T_a, I_0) + \psi(T_{TBR}, T_s) \tag{7a}$$

where the term $\phi(T_{TBR}, T_a, I_0)$ is equal to the temperature dynamics for a closed PBR with no inflow (3) and stands for the natural thermal dynamics of the reactor. The term $\psi(T_{TBR}, T_s)$ represents the heat flow from the temperature regulation system. Here, the temperature regulation is represented

by a simple linear controller:

$$\psi(T_{TBR}, T_s) = \delta_{HE}(T_{TBR})[K_p(T_s - T_{TBR}) - \phi(T_{TBR}, T_a, I_0)] \tag{7b}$$

$$\delta_{HE}(T_{TBR}) = \begin{cases} 1 & \text{if } T_{TBR} \leq T_s - \epsilon, \\ \frac{T_s + \epsilon - T_{TBR}}{2\epsilon} & \text{if } T_s - \epsilon < T_{TBR} < T_s + \epsilon \\ 0 & \text{if } T_{TBR} \geq T_s + \epsilon, . \end{cases} \tag{7c}$$

$$(\epsilon = 0.2^{\circ}\mathrm{C})$$

$$T_s = \theta_4\ 27.5 + 273.15 \tag{7d}$$

where S_{TBR} is the surface area ($36.4\,\mathrm{m}^2$). While addressing the challenges posed by the SATHE model, it is imperative to validate its performance under real-world conditions.

3.3. Validation: performance-evaluation of the SATHE model predicting the temperature in a TBR

In this section, we present the results of the temperature prediction model outlined in (7). Fig. 3 illustrates the temperature prediction following a 4-day calibration phase. For 14 days, the average absolute error in temperature prediction is 1.43 °C.However, for long-term predictions (as depicted in Fig. 3), it is important to acknowledge that numerous system variables may change, leading to a reduction in prediction performance. This can be attributed to factors such as variations in greenhouse temperature or adjustments in external controls. The prediction model's performance can be enhanced through readjusting the parameters.

Beyond day 84, a notable shift is observed in the minimum temperature of the medium. It transitions from 27.5 °C to 26 °C. The subsequent readaptation of parameters, as demonstrated in Fig. 4, showcases the corresponding improvement in prediction performance.

A key feature of the model is its ability to predict temperature using minimal data, specifically from nearby weather stations, without the need for additional sensors (apart from 4 days of data from inside the reactor). This has several benefits, such as reducing costs related to additional sensors, as well as saving manpower required to maintain these sensors and handle their data. By relying primarily on in-reactor measurements and weather data, the model becomes less dependent on specific in-greenhouse measurements.

However, with higher data quality for the light I_0 and ambient temperature T_a, the calibration and the prediction quality improve. In Fig. 5, we

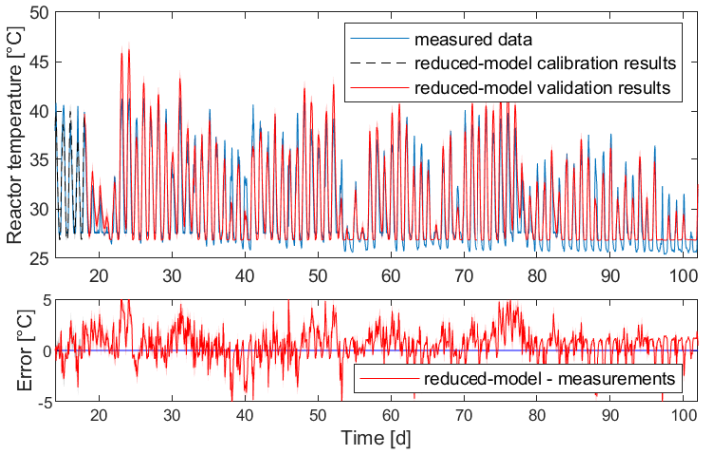

Figure 3: Using a data set of 4 days to fit the SATHE model. Model simulations (red line) vs records (blue line). Model predictions start from day 14.

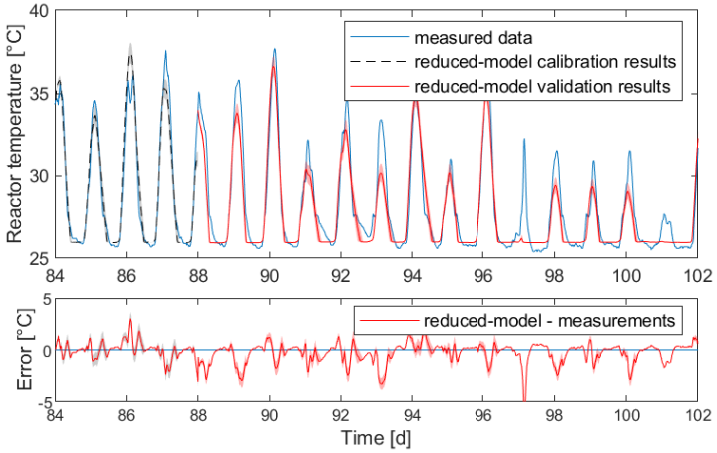

Figure 4: Using a data set of 4 days to fit the SATHE model. Model simulations (red) vs records (blue line) from the TBR upon day 84.

use the air temperature from inside the greenhouse and data from the light sensors that are attached to the reactor (see Fig. 1). The most visible difference is at day 97. The average absolute error for a 14 days prediction drops from 0.6859 °C in Fig. 4 to 0.4103 °C Fig. 5 by using more precise data.

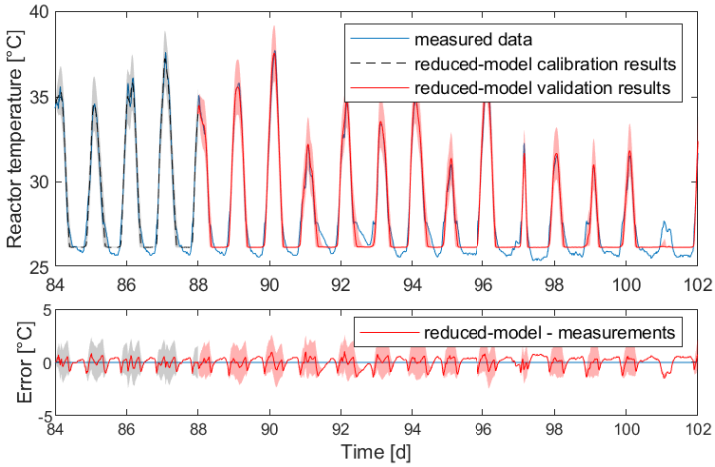

Figure 5: Using records from 4 days of probes inside the greenhouse (temperature) and in the TBR (PAR) to fit the SATHE model. Model (red line) vs measurements (blue line) from the TBR upon day 84.

There is a trade-off between cost, accuracy, and practicality. While on-site sensors improve precision, the model's ability to use only weather station and in-reactor data makes it practical for broader applications, especially where cost reduction is essential. Using additional sensors offers better accuracy but comes at higher costs.

4. Applying the SATHE Model to a V-shape PBR

4.1. Description of the V-shape reactor

Flat panel reactors are enclosed systems, using flat, transparent panels. They offer controlled conditions for efficient growth and are designed to maximize surface area for cultivation (Carvalho et al., 2006). The V-shaped PBR, based in Bonaire (part of the Lesser Antilles in the southern Caribbean Sea) represents a significant advancement in microalgae cultivation, particularly in terms of optimizing light distribution and temperature control. This innovative design, presented by Chin-On et al. (2022), proposes a vertical

orientation of panels, effectively increasing the surface area exposed to light. By doing so, light is diluted and reflected, ensuring that microalgae receive an optimal light intensity within the range they are naturally adapted to (50-200 µmolph/m^2/s). This distribution not only enhances potential areal productivity but also minimizes light loss by trapping and reflecting it back onto the culture, a feature absent in traditional flat-panel reactors.

The V-shaped PBR setup involves two plates configured in a V-shape, with specific inclinations for the north and south panels. The inclination angles, as illustrated in Fig. 6, are set at 80° for the north panel and 70° for the south panel. These angles are strategically chosen to optimize light exposure based on the geographical location. The north panel is oriented to face directly south, while the opposite applies to the south panel. This setup ensures that both panels receive high light availability throughout the day (Chin-On et al., 2022).

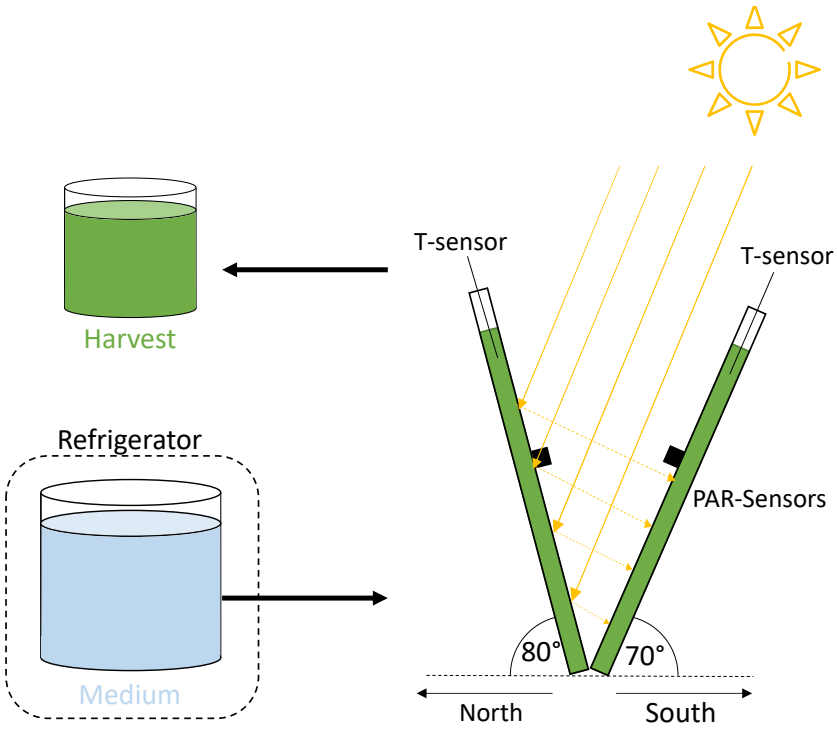

Figure 6: Schematic of the V-shaped reactor, illustrating sunlight reflectance on both (tilted) panels. The positions of the light sensor (PAR sensor) and temperature sensor (T sensor) on each panel are indicated, along with the supply of fresh, cooled medium.

Each of the panels is equipped with a separate recirculation circuit. This setup is crucial for testing both panels individually, as they are exposed to different light intensities. Additionally, integrated sensors continuously monitor various parameters such as temperature, photosynthetically active radiation (PAR), dissolved oxygen levels, pH, turbidity, and flow rates.

The reactor was operated in two operation modes. In the repeated batch mode, a series of discrete batches of microalgae culture were sequentially introduced into the reactor. Each batch was allowed to grow until it reached a specified biomass concentration, after which it was harvested and replaced with a fresh batch. Daily procedures in this mode involved dilution and replenishment of the reactor contents at 15:00 hours. A pre-determined volume of the culture was harvested, and the reactor was refilled with fresh medium. After 15 minutes of circulation with the freshly filled reactor, another sample was collected.

In contrast, the chemostat mode represents a continuous cultivation approach. Here, cooled medium is continuously added to the reactor while an equivalent volume is simultaneously withdrawn to maintain a constant culture volume. This design principle not only maximizes light utilization but also addresses temperature regulation, crucial for sustaining optimal growth conditions.

Accurately modelling temperature within the V-shaped PBR helps in predicting and optimizing microalgae cultivation, enabling efficient thermal management and assessing the need for additional heat control. Furthermore, this modelling of diverse weather conditions assists in the selection of appropriate microalgae species tailored to specific geographical locations.

4.2. Explaining the hypothesis for the SATHE model to adapt to the V-shape reactor

Instead of having a horizontal flat surface, this reactor has a V-shape to profit from reflections from incoming light. Weather stations however deliver light for horizontal surfaces. Since the V-shape reactor panels' surfaces are inclined, the inaccuracy of incoming light compared to a flat surface can be a hurdle for the SATHE model. The reactor is equipped with light sensors (see Fig. 6). As depicted in Fig. 7, it's evident that the incoming light varies significantly between the two panels.

While the adaptive model is intended to forecast reactor temperatures based on weather data, in this instance, such data were not accessible. Instead, we rely on temperature and light information from ambient sensors

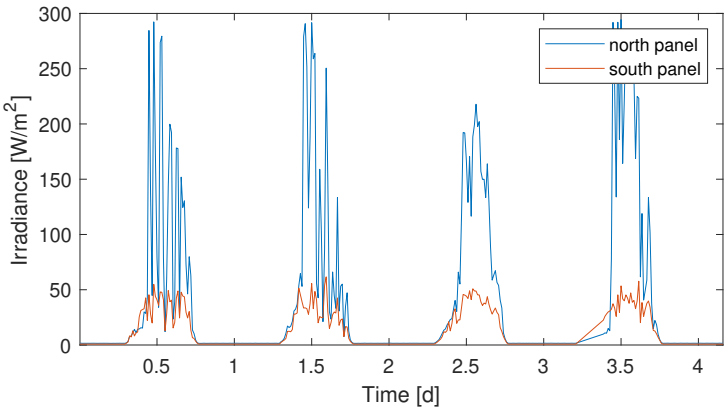

Figure 7: Incoming light irradiance at the centre of the panels of the V-shape reactor.

next to the reactor location. The light sensor measures the light on a flat surface, which is equivalent to the data, a weather station provides.

This discrepancy in incoming light, as illustrated in Fig. 7, may contribute to the observed temperature differential within both panels (see Fig. C.14). This conclusion is supported by the consistent temperature measurements taken within the medium of both the north and south panels. Therefore we calibrate the two sets separately.

In chemostat mode, the consistent flow rate from the vessel to the panels is at $0.53\,\mathrm{d}^{-1}$. The medium is refrigerated, but the actual temperature of the medium (4 °C to 6 °C) is not monitored. We assume the inflow temperature to be at 5 °C. For the chemostat mode, we apply the SATHE model in (2).

In repeated batch mode, the medium was stored outside and had ambient temperature. For that mode, we imply the model in (Appendix A). The volume inside the reactor was constant at $V_{Vshape} = 0.0815\,\mathrm{m}^3$ for both experimental runs and the surface $S_{Vshape} = 1.041\,\mathrm{m}^2$.

4.3. Validation: performance-evaluation of the SATHE model predicting the temperature in the V-shape reactor

In this section, we present the results of predicting temperature following a dedicated 4-day calibration phase for model parameterization. Fig. 8 and Fig. C.13 showcase the model's accuracy in predicting temperature for the repeated batch in both panels and under the ambient temperatures given in Fig. C.15, which is around 15 °C above the temperatures outside the greenhouse in Wageningen (see Fig. 2).

The average absolute error is at 0.3708 ° C over a 30-day prediction period. It is worth noting that in Fig. 8, the peaks correspond to instances where the temperature sensor was temporarily removed from the panel for calibrating the pH probe, around 15:00 hours.

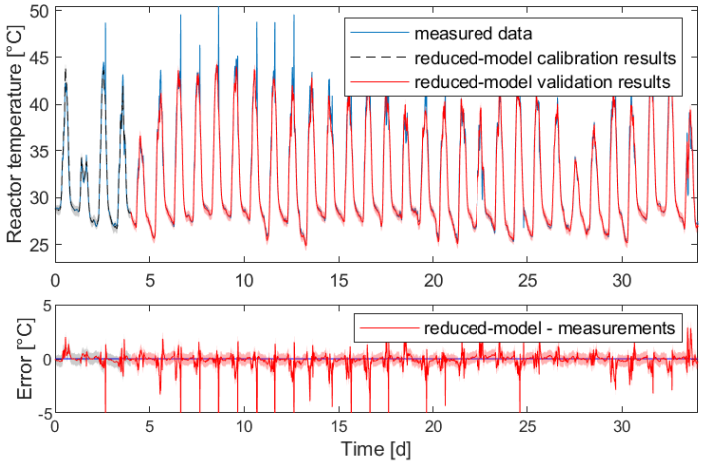

Figure 8: Using a data set of 4 days to fit the SATHE model. Model predictions (red line) vs measurements (blue line) of the north panel of the V-shape reactor operated in repeated batch.

Similarly, Fig. C.16 and Fig. C.17 present the accurate temperature predictions provided by the model for the chemostat. These plots demonstrate the model's high level of accuracy, with the absolute error not exceeding 2.2 °C.

The results show that the model can accurately predict temperature changes in various cultivation systems, including closed setups like the TBR and the V-shaped PBR, even in greenhouse conditions. After validating the model, we can now examine its practical applications in the next section, where we'll examine its capabilities in real-world scenarios.

5. Scenario Simulations: Energy and Temperature under Varying Conditions

Measuring temperature in a microalgal reactor is straightforward and relies on cheap and reliable sensors, which are most of the time implemented together with other probes (pH, oxygen,...). Calibrating the SATHE model

from a large number of data is thus mainly depending on the accuracy of the meteorological information. The study of the TBR showed that measuring locally the climate is the most accurate option. However, there are currently easy accesses to weather data bases for feeding the model. This is the main interest of our approach to offer a prediction of the future medium temperature once weather forecasts are available. In the first case study with the TBR, we demonstrate that the temperature can be accurately predicted using the weather measurements of a meteorological station located 17 km away. In this case, the SATHE model, through the adaptation of the θ_i parameters, also compensates for the difference between the outdoor conditions and the conditions in the greenhouse. This is a striking result that we did not use an intermediate model representing the climate outside the greenhouse. The SATHE model can then be used to support control strategies to (passively) maintain the medium temperature close to the optimum temperature for the algae, and at least always anticipate extreme temperature events which can lead to massive cell mortality. As it was developed in previous works (DeLuca et al., 2017, 2019), such strategies can enhance productivity gains of 50%.

Beyond guiding proactive actions to protect the process against overheating and optimize its efficiency, the model can help in assessing the productivity potential for an outdoor photobioreactor growing a given species in a specific location accounting for its climate. In this section, we explore further applications and advantages of the SATHE model for evaluating the energy required to maintain a process in optimal conditions. Fig. 9 shows recorded weather data for Deelen, Netherlands in June 2023. After calibration, the reduced model includes the basic heat transfer factors between external conditions and the V-shaped reactor. Employing the calibrated model with that weather data the lower plot in Fig. 9 illustrates the temperature evolution within the V-shaped reactor in Deelen during Summer 2023.

The simulation reveals that the reactor temperature drops till around 10 °C. This simulation indicates that Deelen offers less suitable conditions for optimal growth and productivity microalgae cultivation, compared to Bonaire.

In addition to different geographic locations, the SATHE model can be applied to calculate energy consumption in diverse conditions. To maintain optimal temperatures inside the reactor, supplemental heating, as detailed in Section 3, may be necessary. However, TBRs are known for their significant energy usage (Acién et al., 2012, Egbo et al., 2018, Gupta et al., 2015).

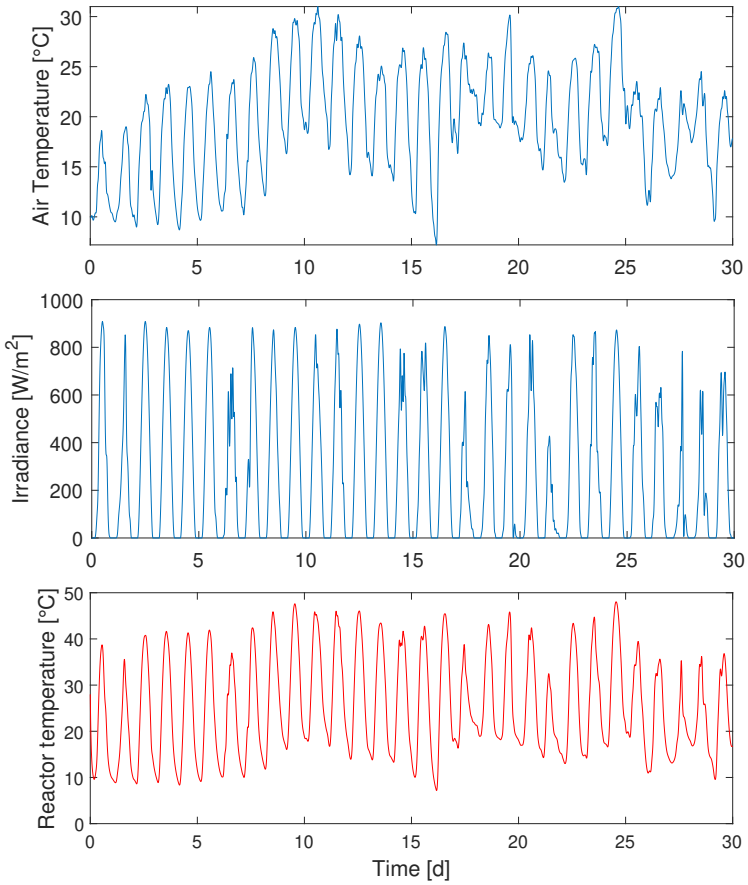

Figure 9: Recorded weather data from the weather station (*upper and middle plot*) and temperature prediction (*lower plot*) of the calibrated SATHE model inside the V-shape reactor in summer 2023 in Deelen (Netherlands).

In the following analysis, we focus on simulating temperature predictions without a heating element. Utilizing the four identified parameters, we employ only the first three θ_1, θ_2, and θ_3 in predicting the temperature. Employing model (3) with these optimized parameters results in the prediction depicted by the grey line in Fig. 10.

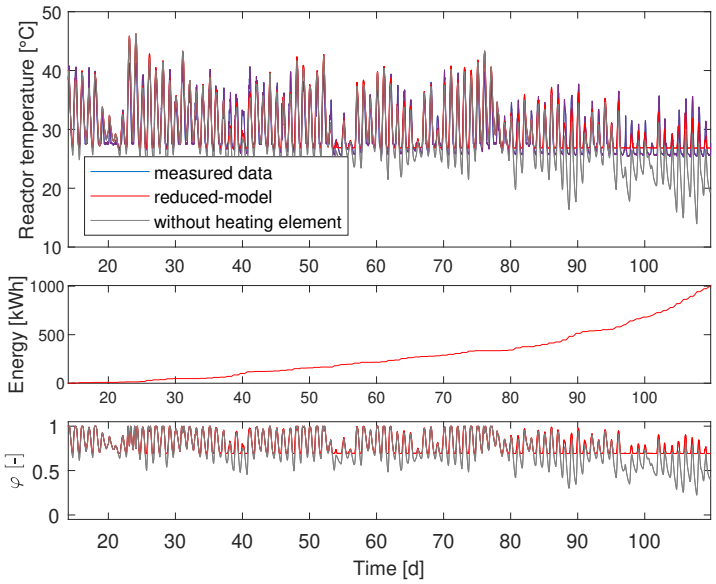

Figure 10: *Upper and middle plot*: Temperature prediction with (red line) and without (grey line) heat exchanger inside the TBR. *Lower plot*: effect of temperature on growth rate as represented by $\varphi(T)$.

The obtained results show that without heating, the temperature drops below 25 °C. *Galdieria sulphuraria* is a strain resistant to higher temperatures and optimal growth is at 40 °C to 42 °C (Náhlík et al., 2021). Considering the model of Bernard and Rémond (2012) describing growth rate as a function of temperature (T) and light (I):

$$\mu(T) = \mu_{\max}\ \varphi(T)\varrho(I)$$

with μ_{max} the maximum specific growth rate.

$$\varphi(T) = \begin{cases} 0, & \text{if } T \leq T_{min} \\ \frac{(T-T_{max})(T-T_{min})^2}{(T_{opt}-T_{min})[(T_{opt}-T_{min})(T-T_{opt})-(T_{opt}-T_{max})(T_{opt}+T_{min}-2T)]}, & \text{if } T_{min} < T \leq T_{max} \\ 0, & \text{if } T > T_{max} \end{cases} \tag{8}$$

Given $T_{min} = 0\,°\text{C}$, $T_{opt} = 39\,°\text{C}$ and $T_{max} = 51.5\,°\text{C}$ (Paerl et al., 2011), the lower plot in Fig. 10 shows that the growth factor $\varphi(T)$ is higher when a heater is used in the reactor. This indicates better growth conditions for microalgae inside the reactor. Temperatures below the optimal range reduce growth productivity, as seen in the decrease of $\varphi(T)$ outside the optimal temperature zone.

However, it is important to consider the energy consumption associated with the heating element. On hotter/warmer days, similar to the ones discussed in this case, energy consumption totals approximately 1000 kWh over 100 days, as evident in Fig. 10. Notably, These calculations do not take into account the energy used for heating the greenhouse. This energy calculation results from integrating the modelled activity of the heat exchanger over time, i.e.,

$$E = \int \psi(T_{TBR}, T_s)\ V_{TBR}\ dt. \tag{9}$$

The adaptive model empowers to simulate temperature predictions and estimate energy consumption for the TBR under diverse weather conditions. Now, we look into an energy consumption analysis of the TBR and additionally consider the same weather conditions that the V-shape reactor in Bonaire undergoes when in repeated batch mode (see Fig. C.13).

Fig. 11 shows the temperature prediction alongside the anticipated energy consumption by the heat exchanger on Bonaire (outside). Over 37 days, the projected consumption would total 187 kWh. In this scenario, we highlight, that there is no additional heating for the greenhouse.

6. Conclusion

This study introduces and validates the SATHE model for predicting temperature within closed PBRs. It demonstrates the model's effectiveness in simulating the temperature in microalgae cultivation systems, which can

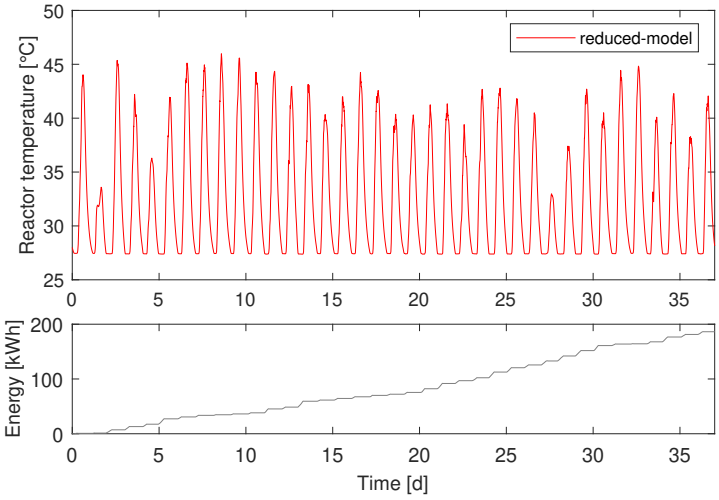

Figure 11: Temperature prediction for Bonaire's climate together with energy consumption of the heat exchanger inside the TBR.

be further integrated within a productivity model. Through rigorous validation against real-world closed reactors, the model demonstrates its ability to accurately predict reactor temperatures, which is crucial for optimizing microalgae growth conditions. This model can thus be used, in the same spirit as De-Luca et al. (2017, 2019) in a Model Predictive Control (MPC) framework for anticipating the consequence of the future weather in the process management. Such proactive actions based on weather forecats can help to maintain the reactor temperature in an optimal window for the algal growth. Furthermore, its flexibility in simulating varying environmental conditions emphasizes its potential for geographical and species selection. The results highlight the challenges posed by varying weather conditions in certain regions, showing the limitations of cultivating microalgae within specific simulated climates. The model can help to better assess the energy consumption, particularly in colder climates, along the year, and provide data for a more accurate Life Cycle Assessment.

In future work, leveraging the model's adaptability paves the way for its integration into real-time control strategies like Optimal and Model Predictive Control (MPC).

Figure	**Reactor**	**Cali. days (further info.)**	***RMSE* over a prediction span of d days**				***MAE* over a prediction span of d days**			
			$d = 1$	$d = 4$	$d = 14$	$d = all$	$d = 1$	$d = 4$	$d = 14$	$d = all$
Fig. 3	TBR	14-18 (data from outside GH)	1.654	1.557	1.834	1.558	1.388	1.311	1.432	1.202
Fig. 4	TBR	84-88 (data from outside GH)	1.073	1.023	1.029	1.135	0.730	0.722	0.684	0.739
Fig. 5	TBR	84-88 (data from inside GH)	0.402	0.458	0.496	0.498	0.315	0.374	0.411	0.418
Fig. C.13	V-shape (S)	0-4 (rep. batch)	0.734	0.546	0.538	0.568	0.450	0.357	0.361	0.385
Fig. 8	V-shape (N)	0-4 (rep. batch)	0.376	0.819	1.004	0.815	0.255	0.382	0.441	0.410
Fig. C.16	V-shape (S)	0-4 (chemostat)	0.449	0.543		0.545	0.317	0.370		0.387
Fig. C.17	V-shape (N)	0-4 (chemostat)	0.690	0.578		0.585	0.458	0.378		0.402

Table 2: Temperature error quantification results for all figures: RMSE [°C] and MAE [°C] for the SATHE model (SATHE) and the full-model (Full) for the prediction over $d = 1$ day, $d = 4$ days, $d = 14$ days and till the end ($d = all$) of the respective plot and data set. Specifying the calibration days (cali. days) and further information like the source of weather data (from inside or outside the greenhouse) for the TBR and the cultivation mode for the V-shape reactor.

.

Acknowledgements

This work has received funding from the Digitalgaesation project within the European Union's Horizon 2020 research and innovation program under the Marie Skłodowska-Curie grant agreement No. 955520.

References

Abiusi, F., Moñino Fernández, P., Canziani, S., Janssen, M., Wijffels, R.H., Barbosa, M., 2022. Mixotrophic cultivation of Galdieria sulphuraria for C-phycocyanin and protein production. Algal Research 61, 102603. doi:10.1016/j.algal.2021.102603.

Acién, F., Fernández, J., Magán, J., Molina, E., 2012. Production cost of a real microalgae production plant and strategies to reduce it. Biotechnology Advances 30, 1344–1353. doi:10.1016/j.biotechadv.2012.02.005.

Acién, F., Molina, E., Reis, A., Torzillo, G., Zittelli, G., Sepúlveda, C., Masojídek, J., 2017. Photobioreactors for the production of microalgae, in: Microalgae-Based Biofuels and Bioproducts. Elsevier, pp. 1–44. doi:10.1016/B978-0-08-101023-5.00001-7.

Alavijeh, R.S., Karimi, K., Wijffels, R.H., Van Den Berg, C., Eppink, M., 2020. Combined bead milling and enzymatic hydrolysis for efficient fractionation of lipids, proteins, and carbohydrates of Chlorella vulgaris microalgae. Bioresource Technology 309, 123321. doi:10.1016/j.biortech.2020.123321.

Béchet, Q., Shilton, A., Park, J.B.K., Craggs, R.J., Guieysse, B., 2011. Universal Temperature Model for Shallow Algal Ponds Provides Improved Accuracy. Environ. Sci. Technol. 45, 3702–3709. doi:10.1021/es1040706.

Bernard, O., Rémond, B., 2012. Validation of a simple model accounting for light and temperature effect on microalgal growth. Bioresource Technology 123, 520–527. doi:10.1016/j.biortech.2012.07.022.

Borowitzka, M.A., 1999. Commercial production of microalgae: ponds, tanks, tubes and fermenters. Journal of Biotechnology 70, 313–321. doi:10.1016/S0168-1656(99)00083-8.

Carvalho, A.P., Meireles, L.A., Malcata, F.X., 2006. Microalgal Reactors: A Review of Enclosed System Designs and Performances. Biotechnol Progress 22, 1490–1506. doi:10.1002/bp060065r.

Casagli, F., Bernard, O., 2022. Coupling heat transfer modelling to ALBA model for full predictions from meteorology. IFAC-PapersOnLine 55, 558–563. doi:10.1016/j.ifacol.2022.09.154.

Casagli, F., Rossi, S., Steyer, J.P., Bernard, O., Ficara, E., 2021. Balancing Microalgae and Nitrifiers for Wastewater Treatment: Can Inorganic Carbon Limitation Cause an Environmental Threat? Environ. Sci. Technol. 55, 3940–3955. doi:10.1021/acs.est.0c05264.

Chin-On, R.C., Barbosa, M.J., Wijffels, R.H., Janssen, M., 2022. A novel V-shaped photobioreactor design for microalgae cultivation at low latitudes: Modelling biomass productivities of Chlorella sorokiniana on Bonaire. Chemical Engineering Journal 449, 137793. doi:10.1016/j.cej.2022.137793.

De-Luca, R., Bezzo, F., Béchet, Q., Bernard, O., 2017. Exploiting meteorological forecasts for the optimal operation of algal ponds. Journal of Process Control 55, 55–65. doi:10.1016/j.jprocont.2017.03.010.

De-Luca, R., Bezzo, F., Béchet, Q., Bernard, O., 2019. Meteorological Data-Based Optimal Control Strategy for Microalgae Cultivation in Open Pond Systems. Complexity 2019, 1–12. doi:10.1155/2019/4363895.

Egbo, N.M., Okoani, A., Okoh, I., 2018. Photobioreactors for microalgae cultivation-an overview. Int J Sci Eng Res 9, 65–74.

Gharib, A., Djema, W., Casagli, F., Bernard, O., 2023. An auto-adaptive heat transfer model predicting the temperature evolution in photobioreactors. IFAC-PapersOnLine 56, 9715–9720. doi:10.1016/j.ifacol.2023.10.284.

Gharib, A., Djema, W., Casagli, F., Bernard, O., 2024. Adaptive temperature model for microalgae cultivation systems. Journal of Process Control 141, 103280. doi:10.1016/j.jprocont.2024.103280.

Goetz, V., Le Borgne, F., Pruvost, J., Plantard, G., Legrand, J., 2011. A generic temperature model for solar photobioreactors. Chemical Engineering Journal 175, 443–449. doi:10.1016/j.cej.2011.09.052.

Guimarães, B.O., De Boer, K., Gremmen, P., Drinkwaard, A., Wieggers, R., H. Wijffels, R., J. Barbosa, M., D'Adamo, S., 2021. Selenium enrichment in the marine microalga Nannochloropsis oceanica. Algal Research 59, 102427. doi:10.1016/j.algal.2021.102427.

Gupta, P.L., Lee, S.M., Choi, H.J., 2015. A mini review: photobioreactors for large scale algal cultivation. World J Microbiol Biotechnol 31, 1409–1417. doi:10.1007/s11274-015-1892-4.

Huang, Q., Jiang, F., Wang, L., Yang, C., 2017. Design of Photobioreactors for Mass Cultivation of Photosynthetic Organisms. Engineering 3, 318–329. doi:10.1016/J.ENG.2017.03.020.

Jacob-Lopes, E., Maroneze, M.M., Queiroz, M.I., Zepka, L.Q., 2020. Handbook of microalgae-based processes and products: Fundamentals and advances in energy, food, feed, fertilizer, and bioactive compounds. Academic Press.

Kumar, M., Sun, Y., Rathour, R., Pandey, A., Thakur, I.S., Tsang, D.C.W., 2020. Algae as potential feedstock for the production of biofuels and value-added products: Opportunities and challenges. Science of The Total Environment 716, 137116. doi:10.1016/j.scitotenv.2020.137116.

Moñino Fernández, P., Vidal García, A., Jansen, T., Evers, W., Barbosa, M., Janssen, M., 2023. Scale-down of oxygen and glucose fluctuations in a tubular photobioreactor operated under oxygen-balanced mixotrophy. Biotech & Bioengineering 120, 1569–1583. doi:10.1002/bit.28372.

Náhlík, V., Zachleder, V., Čížková, M., Bišová, K., Singh, A., Mezricky, D., Řezanka, T., Vítová, M., 2021. Growth under Different Trophic Regimes and Synchronization of the Red Microalga Galdieria sulphuraria. Biomolecules 11, 939. doi:10.3390/biom11070939.

Paerl, H.W., Hall, N.S., Calandrino, E.S., 2011. Controlling harmful cyanobacterial blooms in a world experiencing anthropogenic and climatic-induced change. Science of The Total Environment 409, 1739–1745. doi:10.1016/j.scitotenv.2011.02.001.

Pruvost, J., Le Gouic, B., Lepine, O., Legrand, J., Le Borgne, F., 2016. Microalgae culture in building-integrated photobioreactors: Biomass pro-

duction modelling and energetic analysis. Chemical Engineering Journal 284, 850–861. doi:10.1016/j.cej.2015.08.118.

Ras, M., Steyer, J.P., Bernard, O., 2013. Temperature effect on microalgae: a crucial factor for outdoor production. Rev Environ Sci Biotechnol 12, 153–164. doi:10.1007/s11157-013-9310-6.

Ruiz, J., Olivieri, G., De Vree, J., Bosma, R., Willems, P., Reith, J.H., Eppink, M.H.M., Kleinegris, D.M.M., Wijffels, R.H., Barbosa, M.J., 2016. Towards industrial products from microalgae. Energy Environ. Sci. 9, 3036–3043. doi:10.1039/C6EE01493C.

Serra-Maia, R., Bernard, O., Gonçalves, A., Bensalem, S., Lopes, F., 2016. Influence of temperature on Chlorella vulgaris growth and mortality rates in a photobioreactor. Algal Research 18, 352–359. doi:10.1016/j.algal.2016.06.016.

Singh, S.P., Singh, P., 2015. Effect of temperature and light on the growth of algae species: A review. Renewable and Sustainable Energy Reviews 50, 431–444. doi:10.1016/j.rser.2015.05.024.

Todisco, E., Louveau, J., Thobie, C., Dechandol, E., Hervé, L., Durécu, S., Titica, M., Pruvost, J., 2022. A dynamic model for temperature prediction in a façade-integrated photobioreactor. Chemical Engineering Research and Design 181, 371–383. doi:10.1016/j.cherd.2022.03.017.

Wang, B., Lan, C.Q., Horsman, M., 2012. Closed photobioreactors for production of microalgal biomasses. Biotechnology Advances 30, 904–912. doi:10.1016/j.biotechadv.2012.01.019.

Appendix A. PBR with inflow: Sensitivity function

Due to the reduced number of parameters in the model, the sensitivity functions used in the optimization process were modified accordingly, so the corresponding equation for the sensitivity function becomes

$$\frac{d}{dt}\left(\frac{\partial y}{\partial \theta}\right) = [\dot{\sigma}_T] = \left[\begin{array}{c} \frac{\partial \dot{T}_R}{\partial T_R} \end{array}\right][\sigma_T] + \left[\frac{\partial \dot{T}_R}{\partial \theta}\right] \tag{A.1}$$

where the Jacobian matrix entry is given by

$$\frac{\partial \dot{T}_R}{\partial T_R} = \frac{S_R}{V_R}\left(4\theta_1\lambda_2 T_R^3 - q_{in}\right) \tag{A.2}$$

and partial derivatives of the state with respect to the parameters are

$$\left[\begin{array}{c} \dfrac{\partial \dot{T}_R}{\partial \theta} \end{array}\right] = \left[\begin{array}{ccc} \frac{S_R\lambda_2 T_R^4}{V_R}, & \frac{S_R\lambda_4 T_a^4}{V_R}, & \frac{S_R\lambda_5 I_0}{V_R} \end{array}\right]. \tag{A.3}$$

Appendix B. PBR without inflow: Sensitivity function

Due to the reduced number of parameters in the model, the sensitivity functions used in the optimization process were modified accordingly, so the corresponding equation for the sensitivity function becomes

$$\frac{d}{dt}\left(\frac{\partial y}{\partial \theta}\right) = [\dot{\sigma}_T] = \left[\begin{array}{c} \dfrac{\partial \dot{T}_R}{\partial T_R} \end{array}\right][\sigma_T] + \left[\frac{\partial \dot{T}_R}{\partial \theta}\right] \tag{B.1}$$

where the Jacobian matrix entry is given by

$$\frac{\partial \dot{T}_R}{\partial T_R} = \frac{S_R}{V_R}\left(4\theta_1\lambda_2 T_R^3\right) \tag{B.2}$$

and partial derivatives of the state with respect to the parameters are

$$\left[\begin{array}{c} \dfrac{\partial \dot{T}_R}{\partial \theta} \end{array}\right] = \left[\begin{array}{ccc} \frac{S_R\lambda_2 T_R^4}{V_R}, & \frac{S_R\lambda_4 T_a^4}{V_R}, & \frac{S_R\lambda_5 I_0}{V_R} \end{array}\right]. \tag{B.3}$$

Appendix C. V-shape reactor: additional plots

Appendix D. Optimised parameters

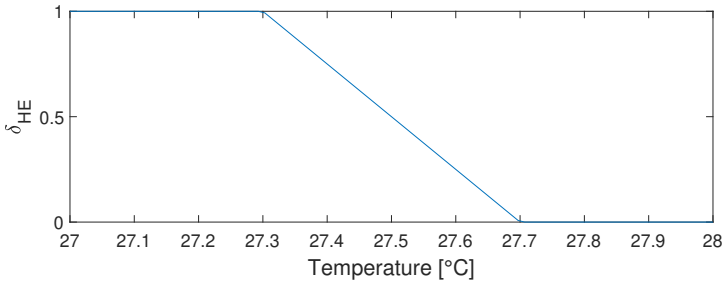

Figure C.12: Heater term trigger. $T_s = 27.5°C$ and $\epsilon = 0.2$

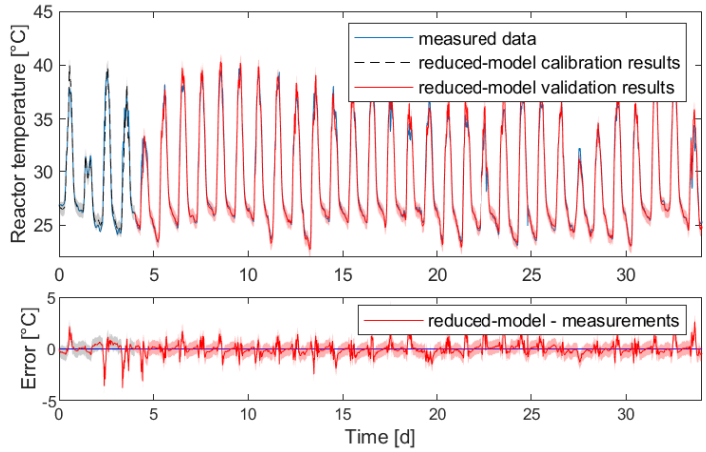

Figure C.13: Using a data set of 4 days to fit the SATHE model. Predictions (red line) vs measurements (blue line) of the south panel of the V-shape reactor operated in repeated batch.

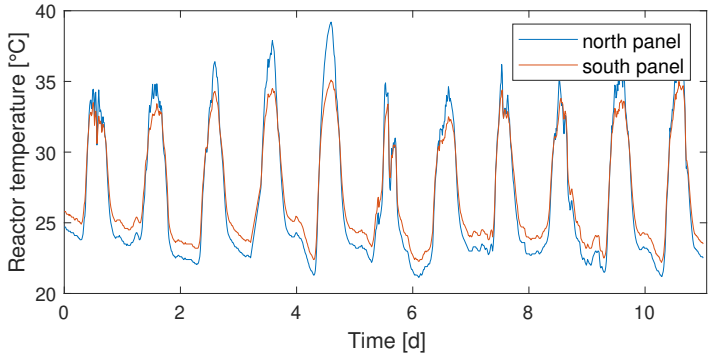

Figure C.14: Measured temperature in both panels of the V-shape reactor.

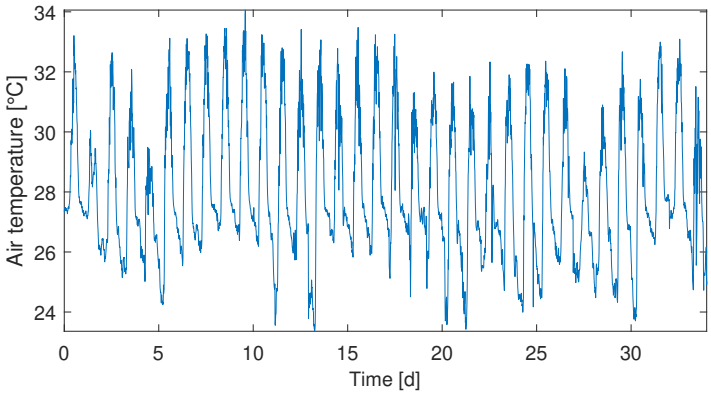

Figure C.15: Ambient temperature for Bonaire, during the period where the reactor was operated in repeated batch mode.

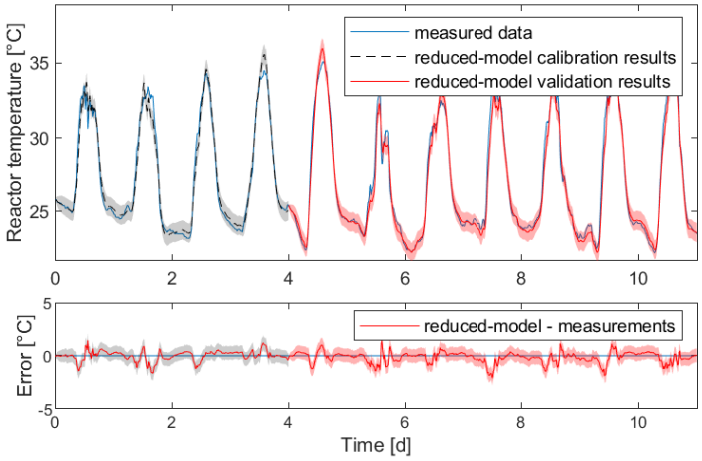

Figure C.16: Using a data set of 4 days to fit the SATHE model. Model predictions (red line) vs records (blue line) of the south panel of the V-shape reactor operated in chemostat.

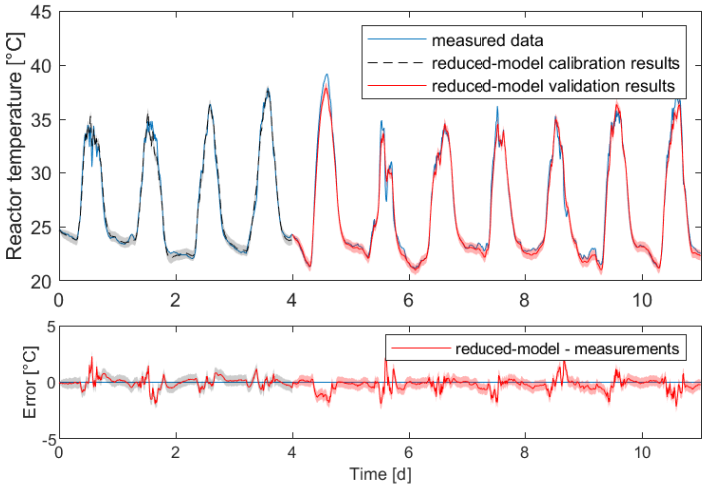

Figure C.17: Using a data set of 4 days to fit the SATHE model. Predictions (red line) vs measurements (blue line) of the north panel of the V-shape reactor operated in chemostat.

	θ_1	θ_2	θ_3	θ_4
Fig. 3	1.295	1.832	0.193	0.980
Fig. 4	1.022	1.404	0.214	0.948
Fig. 5	4.475	5.702	2.114	0.956
Fig. C.13	14.860	18.353	2.231	
Fig. 8	1.838	2.336	0.341	
Fig. C.16	12.755	15.742	1.436	
Fig. C.17	1.806	2.195	0.305	

Table D.3: Calibrated values of parameters θ_i in the various trials presented in figures 3 to C.17